

# Field-effect electroluminescence in silicon nanocrystals

ROBERT J. WALTERS<sup>1\*</sup>, GEORGE I. BOURIANOFF<sup>2</sup> AND HARRY A. ATWATER<sup>1</sup>

<sup>1</sup>Thomas J. Watson Laboratories of Applied Physics, MS 128-95, California Institute of Technology, Pasadena, California 91125, USA

<sup>2</sup>1501 S. MOPAC Exp., MS 4A15, Austin, Texas 78746, USA

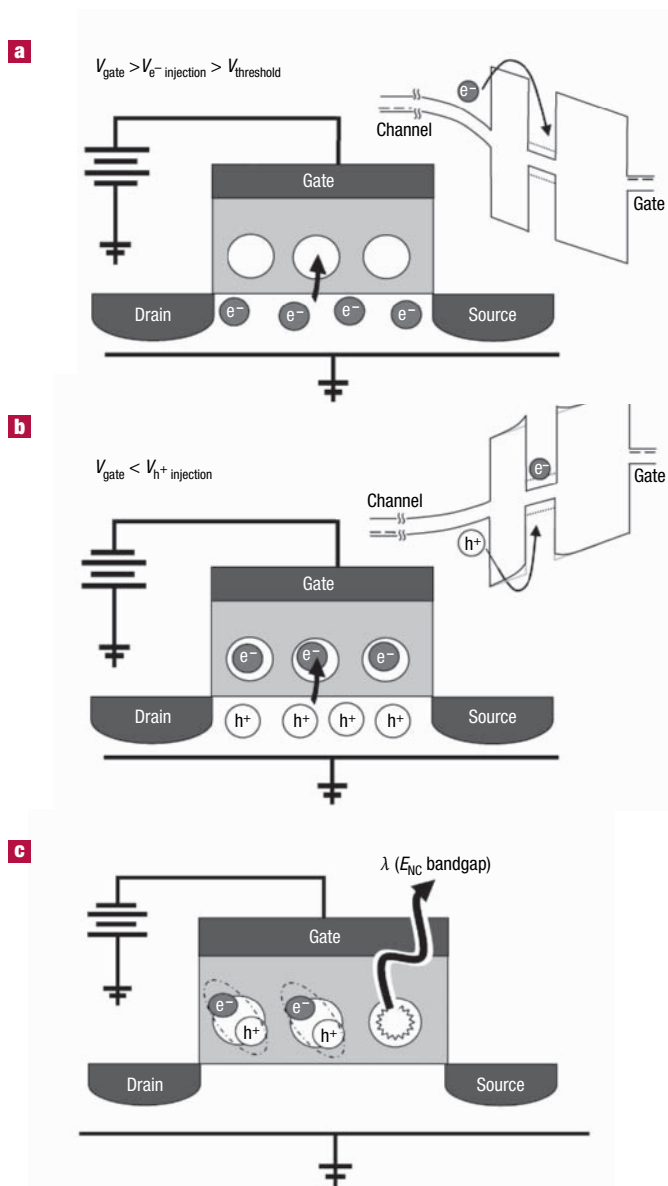
\*e-mail: rwalters@caltech.edu

Published online: 23 January 2005; doi:10.1038/nmat1307

There is currently worldwide interest in developing silicon-based active optical components in order to leverage the infrastructure of silicon microelectronics technology for the fabrication of optoelectronic devices. Light emission in bulk silicon-based devices is constrained in wavelength to infrared emission, and in efficiency by the indirect bandgap of silicon<sup>1,2</sup>. One promising strategy for overcoming these challenges is to make use of quantum-confined excitonic emission in silicon nanocrystals. A critical challenge for silicon nanocrystal devices based on nanocrystals embedded in silicon dioxide has been the development of a method for efficient electrical carrier injection<sup>3–8</sup>. We report here a scheme for electrically pumping dense silicon nanocrystal arrays by a field-effect electroluminescence mechanism. In this excitation process, electrons and holes are both injected from the same semiconductor channel across a tunnelling barrier in a sequential programming process, in contrast to simultaneous carrier injection in conventional pn-junction light-emitting-diode structures. Light emission is strongly correlated with the injection of a second carrier into a nanocrystal that has been previously programmed with a charge of the opposite sign.

A schematic representation of the field-effect electroluminescence mechanism is shown in Fig. 1. The phenomenon is observed in a structure resembling a nanocrystal floating-gate metal-oxide-semiconductor (MOS) transistor memory<sup>9</sup> with two important distinctions. First, the floating-gate array of silicon nanocrystals is formed from well-passivated silicon nanocrystals small enough to have excitonic emission energies that are higher than the bulk silicon emission energy. Secondly, the gate contact is semitransparent at the device emission wavelength but still provides uniform control of the channel potential. Under appropriate bias conditions, the nanocrystal array can be programmed with electrons from an inversion layer or with holes from the channel in accumulation.

**Figure 1** Schematic of the field-effect electroluminescence mechanism in a silicon nanocrystal floating-gate transistor structure. Inset band diagrams depict the relevant tunnelling processes. **a–c**, The array of silicon nanocrystals embedded in the gate oxide of the transistor can be sequentially charged with electrons (**a**) by Fowler–Nordheim tunnelling, and holes (**b**) via Coulomb field-enhanced Fowler–Nordheim tunnelling to prepare excitons that radiatively recombine (**c**).



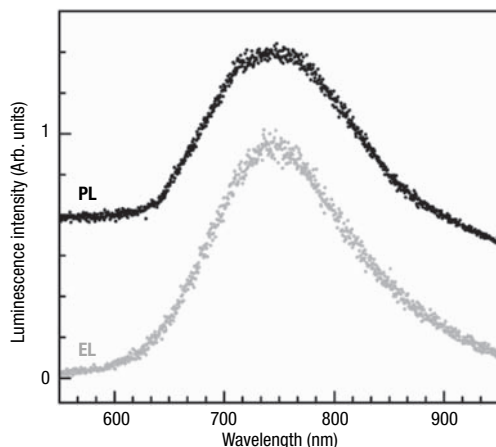


**Figure 2** Photoluminescence (PL) and electroluminescence (EL) emission spectra. Light emission is due to exciton recombination in the array of silicon nanocrystals whether excitons are photoexcited by an ion laser line or created by sequential field-induced carrier injection. The emission spectra are inhomogeneously broadened due to the distribution of luminescent nanocrystal sizes.

As discussed in detail below, excitons can be formed by sequentially programming the nanocrystals with charge carriers of each sign, resulting in electroluminescence. Unlike electroluminescence in bulk light-emitting diodes or previous nanocrystal structures, there is no d.c. current flow.

Figure 2 shows a comparison of nanocrystal photoluminescence (PL) excited through the semitransparent gate contact to nanocrystal electroluminescence (EL). We attribute these spectra to the radiative recombination of excitons within silicon nanocrystals. Both PL and EL spectra peak near 750 nm with full-width at half-maximum of  $\sim 160$  nm. These emission wavelengths are typical for silicon nanocrystals of approximately 2–4 nm in diameter<sup>10</sup>. The spectra are inhomogeneously broadened by the size distribution of silicon nanocrystals in the array.

The electrical excitation process can be understood in more detail by considering the time-resolved electroluminescence trace in Fig. 3. Under negative bias, the p-type channel is in strong accumulation. During this time, the nanocrystal array is charged with holes by Fowler–Nordheim tunnelling across the tunnel oxide. The frequency response suggests that this initial charge-injection process occurs on a timescale of  $\sim 100$   $\mu$ s. When the bias is abruptly changed to a positive voltage above threshold, an electron inversion layer is formed. Electrons are injected into the hole-charged nanocrystals by a Coulomb field-enhanced Fowler–Nordheim tunnelling process, forming quantum-confined excitons. We estimate using Wentzel–Kramer–Brillouin (WKB) approximation-based analysis that a previously injected hole can dramatically enhance the electron tunnelling rate over the Fowler–Nordheim rate for electron tunnelling into a neutral nanocrystal. The onset of electroluminescence is well fit by a single exponential rise ( $\tau \sim 2.5$   $\mu$ s) at the applied 6-V gate bias, suggesting that electron injection is enhanced by a factor of  $\sim 40$  by the presence of holes in the nanocrystal array. This measured electron-tunnelling rate enhancement is consistent with Coulomb field-enhanced Fowler–Nordheim tunnelling through a tunnel oxide thickness of  $\sim 4$  nm, which is the experimental tunnel oxide thickness targeted in our fabrication process. We note that observation of electroluminescence necessarily implies that holes already confined in the nanocrystals have emission times for tunnelling back to the channel that exceed

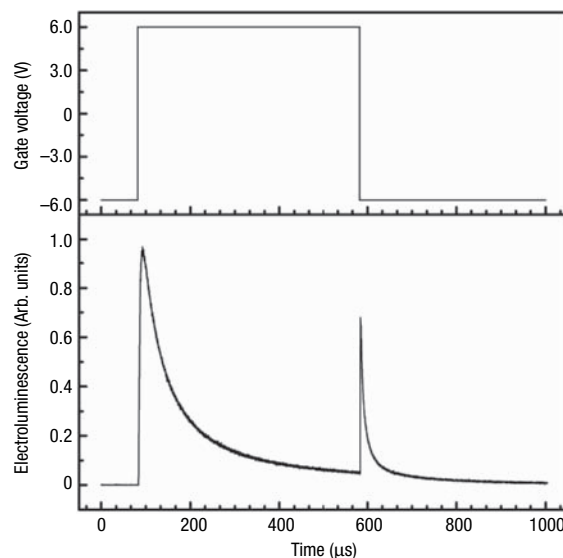


**Figure 3** Time-resolved electroluminescence. Light emission (lower panel) is observed only when the sign of the gate bias (upper panel) is changed, suggesting the mechanism depicted in Fig. 1.

the Coulomb field-enhanced Fowler–Nordheim tunnelling time for electron injection from the inversion layer. The observation of electroluminescence also precludes the injection of multiple electrons into the hole-charged nanocrystals as radiative recombination of excitons is evidently not quenched by Auger recombination, which is known to be an efficient non-radiative recombination mechanism in silicon nanocrystals containing an exciton and an additional charge of either sign<sup>11</sup>.

The emission decays from its peak value as the previously injected holes are consumed by electrons in exciton formation and decay. A stretched exponential equation<sup>12</sup> with a time constant of approximately 30  $\mu$ s ( $\beta \sim 0.5$ ) characterizes the observed decay. This time constant is longer than the photoluminescence decay lifetime observed under optical excitation at an applied gate bias of 6 V ( $\tau \sim 5$   $\mu$ s,  $\beta \sim 0.7$ )<sup>11</sup>. The longer electroluminescence-decay time constant may reflect an absence of non-radiative recombination paths that are present for some fraction of the excitons recombining under illumination. Also, indirect charging processes involving inter-nanocrystal carrier migration could increase the time for exciton formation.

When electroluminescence is no longer observed, there are no more quantum-confined holes left in the array to form excitons. Electrons continue to tunnel into the nanocrystal array due to the positive gate bias, resulting in each nanocrystal becoming recharged with an electron. Multiple charging of nanocrystals is suppressed by Coulombic field-inhibition of Fowler–Nordheim tunnelling into charged nanocrystals. We estimate that the tunnelling rate of second electrons is suppressed by a factor of  $\sim 300$  over the Fowler–Nordheim rate for tunnelling of the first electron into a neutral nanocrystal.

These programmed electrons can now form excitons when the gate voltage is switched to a negative potential sufficient to enable hole injection from the accumulation layer. This process is characterized by a faster single-exponential rise in electroluminescence ( $\tau \sim 240$  ns) and a faster stretched exponential decay ( $\tau \sim 10$   $\mu$ s,  $\beta \sim 0.5$ ). The electroluminescence peak associated with hole injection into electron-charged nanocrystals is smaller in magnitude and shorter in duration than the electroluminescence peak associated with

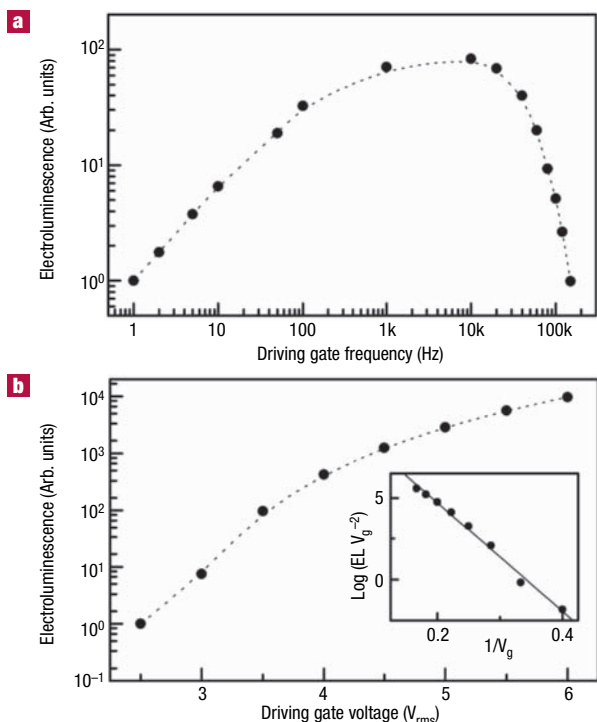


**Figure 4** Variation of electroluminescence intensity. The electroluminescence signal is observed to vary in intensity with: **a**, driving gate frequency, and **b**, gate voltage. The driving frequency was maintained at 10 kHz while the signal magnitude was changed, and the gate voltage magnitude was left at  $6 V_{\text{RMS}}$  while the frequency was changed.

electron injection into hole-charged nanocrystals. We ascribe this asymmetry to stored electron loss by tunnelling back to the channel during hole injection at positive gate bias. This loss mechanism is more apparent for hole injection into electron-charged nanocrystals due to the smaller conduction-band offset ( $\sim 3.2$  eV) than valence-band offset ( $\sim 4.7$  eV) between silicon and silicon oxide.

Electroluminescence is clearly observed to be correlated with injection of the second carrier, indicating that field-effect-induced electroluminescence is due to programmed exciton formation rather than impact excitation resulting from a d.c. leakage current through the gate stack. The lack of emission under d.c. electrical bias is further confirmed by an examination of the frequency dependence of electroluminescence in Fig. 4a. For a constant two-second measurement integration time, electroluminescence is initially observed to increase linearly with increasing driving frequency because light is collected from an increasing number of integrated complete cycles. Electroluminescence emission peaks at a frequency of 10 kHz, and then begins to decrease, which we attribute to several effects. As the driving frequency is increased, the number of excitons formed at positive-to-negative (negative-to-positive) bias transitions begins to decrease due to incomplete initial electron (hole) charging. From the 10-kHz peak in the frequency response, we estimate that charge injection into neutral nanocrystals requires  $\sim 100$   $\mu\text{s}$ . At frequencies above  $\sim 30$  kHz, the pulse duration becomes shorter than the radiative lifetime of silicon nanocrystals and some fraction of the excitons will not recombine. At even higher frequencies, we expect the emission to be further limited by the gate capacitive charging time constant.

As can be seen in Fig. 4b, electroluminescence increases dramatically with increasing r.m.s. drive voltage, and has a

saturation onset at  $\sim 4 V_{\text{RMS}}$ . The tunnel oxide field is proportional to gate voltage and the electroluminescence intensity is proportional to the tunnelling current. Thus we can construct an equivalent Fowler–Nordheim plot (Fig. 4b, inset) that is well fit by a linear relation. This observation is consistent with initial electron and hole injection into neutral nanocrystals being dominated by a Fowler–Nordheim tunnelling process. We expect a distribution of tunnelling oxide barrier thicknesses is present due to the implantation-based nanocrystal formation process. The slope of the Fowler–Nordheim plot is therefore determined by the average value of the effective field strength, which will vary across the array of nanocrystals. Note that the barrier height cannot be determined from the Fowler–Nordheim plot because the average internal quantum efficiency relating the magnitude of the electroluminescence to the tunnelling current is not accurately known.

Field-effect electroluminescence is a general carrier-injection method in which electrons and holes are sequentially injected into a nanocrystal array to form excitons. Silicon nanocrystals and silicon dioxide tunnel barriers might be replaced by other exciton-confining nanostructures or injection-barrier materials. We suggest that devices designed to operate by field-effect electroluminescence be termed field-effect light-emitting devices (FELEDs) as the principle of operation differs significantly from that of pn-junction LEDs, and the resulting device structures resemble field-effect transistors.

FELEDs may be more robust than LED-based nanocrystal light sources because the carrier-injection process can be controlled. In previously reported nanocrystal devices, the optical centres are excited by impact ionization processes in which hot carrier energy creates a nanocrystal-bound exciton<sup>3–6</sup>. In such a process, excess hot carrier energy is lost to thermalization. Over time, excitation by impact ionization degrades the dielectric quality and can lead to oxide wearout and device failure. Field-effect-induced carrier injection may enable the problems associated with impact ionization excitation to be circumvented through controlled Fowler–Nordheim tunnelling. Our FELED test device has so far been observed to be stable over more than  $\sim 5 \times 10^9$  cycles.

## METHODS

Field-effect electroluminescence as described in this report is achieved in MOS transistor structures with optically transparent, doped polysilicon gate electrodes and embedded floating gate arrays of silicon nanocrystals. An initially grown 15-nm-thick dry thermal oxide was implanted with  $^{28}\text{Si}^+$  ions and annealed (5 minutes, 1,050 °C) to precipitate an embedded array of silicon nanocrystals from the supersaturated solid solution. A 40-nm polysilicon layer was then deposited to form a semitransparent gate contact layer. Blanket implantations of  $^{15}\text{P}^+$  and  $^{35}\text{As}^+$  were used to degenerately dope the gate contact, source and drain. Subsequent photoresist patterning and etching were used to form ring-gate MOS-transistor structures. Devices were patterned with electrical contact pads consisting of a 10-nm Cr wetting layer followed by 100 nm of Au using a thermal evaporation and lift-off process and mounted in a Au-wire bonded package. More details of the fabrication process are documented elsewhere<sup>11</sup>. A sketch of the device structure in cross-section appears in Fig. 1. All processing other than metallization and packaging was performed at a 300-mm silicon wafer fabrication facility at Intel Corporation.

Transmission electron microscopy in cross-section was used to confirm the dimensions of the FELED structure. Individual nanocrystals could not be resolved in these images due to low contrast between silicon and  $\text{SiO}_2$ . The presence of Si nanocrystals in the oxide layer was independently verified using ultrahigh vacuum scanning tunnelling microscopy measurements on samples in which the oxide layer of the gate stack was removed with buffered HF (ref. 13). From these measurements, we determine that the areal density of nanocrystals forming the floating gate array is at least  $\sim 4 \times 10^{12}$   $\text{cm}^{-2}$  and that the nanocrystals are  $\sim 2$ – $4$  nm in diameter. A maximum bound on the areal density can be derived from the total fluence of implanted silicon ions and is estimated to be within an order of magnitude of our lower bound. The discrepancy between these bounds may indicate a loss of nanocrystals during the partial etching procedure, a large population of small-diameter ( $< 1$  nm) nanocrystals, and/or a significant loss of material to the bulk during the high-temperature nanocrystal formation anneal<sup>14</sup>. The crystallinity of the nanocrystals was confirmed by the observation of interference rings in reflection high-energy electron diffraction measurements of the etched-back samples<sup>15</sup>.

A numerical one-dimensional WKB approximation was used to compare the tunnelling probabilities and therefore the tunnelling rates of electrons for the Coulomb field-enhanced, Coulomb field-inhibited, and neutral (triangular) Fowler–Nordheim conduction-band tunnel oxide barriers. An exponential thermal distribution was assumed for the electrons in the channel.

A 20-MHz arbitrary function generator with an output termination of 10  $\text{M}\Omega$  was used to electrically pump the packaged FELEDs. Spectra were collected by a grating spectrometer and a cryogenically cooled CCD array using an  $\text{Ar}^+$  ion laser operating at 457.9 nm for optical excitation and

a 10-kHz,  $6-V_{rms}$  square wave for electrical excitation. All spectra were corrected for detector sensitivity. Stray light was removed by optical filters. Time-resolved electroluminescence traces were collected with a thermo-electrically cooled photomultiplier tube and a grating spectrometer. The time-resolved signal is the integrated emission over a passband of approximately 50 nm centred at the emission peak of 750 nm.

Received 10 September 2004; accepted 2 December 2004; published 23 January 2005.

## References

1. Pavesi, L. & Lockwood, D. J. (eds) *Silicon Photonics 1–52* (Topics in Applied Physics Series Vol. 94, Springer, 2004).
2. Green, M. A., Zhao, J., Wang, A., Reece, P. & Gal, M. Efficient silicon light-emitting diodes. *Nature* **412** 805–808 (2001).
3. Valenta, J., Lalic, N. & Linros, J. Electroluminescence of single silicon nanocrystals. *Appl. Phys. Lett.* **84** 1459–1461 (2004).
4. Franzo, G. *et al.* Electroluminescence of silicon nanocrystals in MOS structures. *Appl. Phys. A* **74**, 1–5 (2002).
5. Photopoulos, P. & Nassiopoulou, A. G. Room- and low-temperature voltage tunable electroluminescence from a single layer of silicon quantum dots in between two thin  $\text{SiO}_2$  layers. *Appl. Phys. Lett.* **77**, 1816–1818 (2000).
6. Fujita, S. & Sugiyama, N. Visible light-emitting devices with Schottky contacts on an ultrathin amorphous silicon layer containing silicon nanocrystals. *Appl. Phys. Lett.* **74**, 308–310 (1999).
7. De la Torre, J. *et al.* Optical and electrical transport mechanisms in Si-nanocrystal-based LEDs. *Physica E* **17**, 604–606 (2003).
8. De la Torre, J. *et al.* Optical properties of silicon nanocrystal LEDs. *Physica E* **16**, 326–330 (2003).
9. Hanafi, H. & Tiwari, S. Fast and long retention-time nano-crystal memory. *IEEE Trans. Elec. Dev.* **43**, 1553–1558 (1996).
10. Puzder, A., Williamson, A. J., Grossman, J. C. & Galli, G. Surface control of optical properties in silicon nanoclusters. *J. Chem. Phys.* **117**, 6721–6729 (2002).
11. Walters, R. J. *et al.* Silicon optical nanocrystal memory. *Appl. Phys. Lett.* **85**, 2622–2624 (2004).
12. Linros, J., Lalic, N., Galeckas, A. & Grivickas, V. Analysis of the stretched exponential photoluminescence decay from nanometer-sized silicon crystals in  $\text{SiO}_2$ . *J. Appl. Phys.* **86**, 6128–6134 (1999).
13. Feng, T., Yu, H., Dicken, M., Heath, J. & Atwater, H. A. Probing the size and density of silicon nanocrystals in nanocrystal memory device applications. *Appl. Phys. Lett.* (in the press).
14. Müller, T., Heinig, K.-H. & Möller, W. Nanocrystal formation in Si implanted thin  $\text{SiO}_2$  layers under the influence of an absorbing interface. *Mater. Sci. Eng. B* **101**, 49–54 (2003).

## Acknowledgements

This work was supported by Intel Corporation and the Air Force Office of Scientific Research (#FA9550-04-1-0434). R.J.W. acknowledges National Defense Science and Engineering Graduate Fellowship support through the Army Research Office.

Correspondence and requests for materials should be addressed to R.J.W.

## Competing financial interests

The authors declare that they have no competing financial interests.